Analysis of Ground Effect for Small-Scale UAVs in Forward Flight

Xinyue Kan, Justin Thomas, Hanzhe Teng, Herbert G. Tanner, Vijay Kumar, and Konstantinos Karydis

***Abstract*—The letter investigates how the behavior of small-scale unmanned aerial vehicles (UAVs) is influenced by the system's close proximity to the ground/rigid surfaces both at hover and in forward flight. We perform an extensive experimental study where a quadrotor is tasked with flying in forward velocities in the range of 0–8 m/s and at altitudes that range between 0.05–0.5 m. Experimental data are used to evaluate four existing ground effect models. Results suggest that existing models for helicopters and in-hover multi-rotors cannot fully describe the forward motion of a quadrotor when it operates close to ground. We introduce two new data-driven models for rotorcraft operating in ground effect both at hover and in forward flight, and evaluate the proposed models with another quadrotor of different size. The proposed models simultaneously consider several operating conditions, which are parameterized by the vehicle's forward velocity and altitude. The models link the thrust produced when operating in ground effect and hovering out of ground effect as forward velocities vary. This information can be incorporated into flight controllers for robust and adaptive UAV flights, and can benefit motion planners for safe and energy efficient near-ground trajectory planning.**

***Index Terms*—Aerial Systems: Mechanics and Control, Calibration and Identification, Performance Evaluation and Benchmarking, Ground Effect, Quadrotors.**

I. Introduction

ROTORCRAFTS experience ground effects when operating in close proximity to rigid surfaces, impacting performance in scenarios such as take off, landing, hovering, and forward flight near ground. Near-ground operations are unavoidable in applications including package delivery [1], plant density estimation [2], cooperative construction [3], and autonomous inventory-taking in large warehouses [4] when utilizing Unmanned Aerial Vehicles (UAVs). The capability to predict the behavior of small-scale UAVs both at hover and in forward flight when operating close to ground can help design more efficient motion planners and controllers for autonomous UAV operation in cluttered environments.

Similar to other aerodynamic effects [5], [6], ground effect can be taken into consideration to generate near-ground energy-efficient trajectories. Operating in ground effect (IGE) can be more energy efficient than operating out of ground effect (OGE) in terms of lift-to-drag ratio [7]. The higher the ratio, the more efficient the vehicle is. In steady-state flight, lift balances the vehicle's weight. However, as the vehicle moves forward, the amount of lift produced decreases due to trailing vortices. When the aircraft operates near ground, the ground alters the airflow and partially blocks the trailing vortices [7]. As such, more lift, as well as less induced drag, is generated, and therefore, less thrust is required in order to balance the drag and maintain a desired forward velocity [7].

For energy-aware motion planning, minimum-energy paths can be found with respect to motor angular velocities [8], [9], since required power and thrust have been found to scale proportionally with the cube and square of angular velocity, respectively [7], [10], [11]. Hence, one can command the vehicle to operate close to a rigid surface at a feasible forward velocity to consume less energy. To this end, it is important to study the relationship between forward velocity, distance from the ground, and corresponding required thrust, in order to understand the power consumption in ground effect.

Besides energetic gains on robotic flight, better understanding of ground effect both at hover and in forward flight can provide useful information for robot motion planning and control. Accurate models for ground effect in forward flight, when linked to a robot's characteristic length (e.g., the propeller radius), can indicate safe distances for vehicles to keep not only from the ground, but also from other vehicles in multi-robot teams (e.g., [12], [13]). This information is important when developing robust and adaptive controllers for applications like autonomous landing [14], perching [15], and high-speed flight in confined spaces [16].

Our work improves the understanding of how proximity to the ground affects the behavior of small-scale rotorcraft UAVs across operating conditions in terms of altitude and forward velocity. This is the first study that captures ground effects through extensive indoor experimentation across several altitudes ($0.05-0.5$ m) and forward velocities ($0-8$ m/s). Data are used to evaluate existing models in the literature, and to help derive new ones that are amenable to control. Existing models are found insufficient to accurately capture ground effect

Manuscript received February 24, 2019; accepted June 27, 2019. Date of publication July 22, 2019; date of current version August 1, 2019. This letter was recommended for publication by Associate Editor F. Ruggiero and Editor J. Roberts upon evaluation of the reviewers' comments. This work was supported in part by ARL under Grant W911NF-08-2-0004, in part by ARO under Grant W911NF-13-1-0350, in part by DARPA under Grant HR001151626 and Grant HR0011516850, and in part by the National Science Foundation under Grant IIS-1724341. *(Corresponding author: Konstantinos Karydis.)*

X. Kan, H. Teng, and K. Karydis are with the Department of Electrical and Computer Engineering, University of California, Riverside, Riverside, CA 92521 USA (e-mail: xkan001@ucr.edu; hteng007@ucr.edu; karydis@ucr.edu).

J. Thomas is with the Exyn Technologies, Philadelphia, PA 19146 USA (e-mail: jthomas@exyntechnologies.com).

H. G. Tanner is with the Department of Mechanical Engineering, University of Delaware, Newark, DE 19716 USA (e-mail: btanner@udel.edu).

V. Kumar is with the Department of Mechanical Engineering and Applied Mechanics, University of Pennsylvania, Philadelphia, PA 19104 USA (e-mail: kumar@seas.upenn.edu).

This letter has supplementary downloadable material available at http://ieeexplore.ieee.org, provided by the authors. The material consists of a video, viewable with PotPlayer. The video demonstrates the experiments we performed with a Hummingbird robot and a Crazyflie robot.

Digital Object Identifier 10.1109/LRA.2019.2929993

in forward flight. To address this gap, our proposed models blend data-driven methods with non-dimensional analysis. The proposed models' structure brings forward clear and intuitive relations between key robot characteristics (rotor induced velocity at hover and propeller radius), and important physical operation quantities (forward velocity and altitude). The models' generalization capability is evaluated with data from another quadrotor of different frame size and mass.

II. Background

Ground effect for conventional helicopters at hover has been studied extensively. When hovering close to ground, rotor thrust increases at constant power. *Cheeseman & Bennett* [17] proposed an analytical model using the method of images. *Hayden* [18] identified the influence of ground effect at hover from experimental observations. Both models relate the thrust generated by a single propeller to the distance from the ground.

The presence of multiple rotors may lead to behaviors that cannot be captured by single-rotor models. Related work [19]–[21] has evaluated single-rotor models for ground effect using quadrotors, and demonstrated the existence of ground effect at higher altitudes than predicted analytically [17]. One possible explanation is the strong flow interactions between multiple rotors [22]. Thus, models for single-rotor vehicles cannot be applied directly to multi-rotor ones.

Recent efforts seek to understand the impact of ground effect in small-scale quadrotors. *Li et al.* [14] presented an improved model to compensate for the increase of thrust in ground effect under constant power, and experimentally demonstrated its efficacy within an altitude controller for autonomous landing. *Sanchez-Cuevas et al.* [23] further considered the influence of rotor placements, flow recirculation, and the central body lift. Models of ground effect for a hovering quadrotor can also be derived through data-driven methods [24] based on the principal orthogonal decomposition (POD) [25] or appropriate low-dimensional stochastic modeling [26]. However, these models apply to hover, and quantify ground effect as a function of altitude. Integrating forward velocity remains a challenge.

In forward flight, ground effects are more complex because of the complicated flow states near the rotor. With a forward velocity, a region of flow recirculation upstream of the rotor is formed, which influences the required power as the forward velocity changes. Hence, rotor performance in ground effect tends to differ between low and high forward velocity. Multiple models have been developed to simulate the flow near rotors [19], [27]–[30]. However, when comparing with experimental results, these models are inadequate to predict in-ground-effect rotor performance for small-scale quadrotors in forward flight. The present letter fills this gap.

III. Data Collection and Analysis

We collect data from two distinct quadrotor UAVs (Fig. 1). The first dataset is from an AscTec Hummingbird, which is used to evaluate existing models and to train our proposed models. The second dataset is from a Bitcraze Crazyflie2.0 which is used to validate our proposed models. Both vehicles are commanded to follow pre-planned trajectories. Flight altitude, forward velocity, and 3D position and orientation are measured at 100 Hz via motion capture. IMU measurements, rotor RPM (for Hummingbird), and motor power consumption (for Crazyflie) are recorded through the vehicles' firmware. For Hummingbird, thrust is computed directly from rotor RPM [31]. For Crazyflie, thrust is converted from motor power consumption via the manufacturer's power-thrust curves.

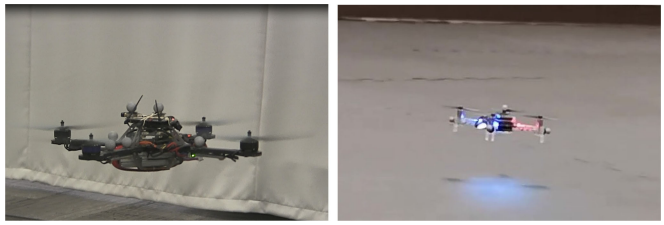

Fig. 1. The quadrotor UAVs used in this study. (Left) Data from an AscTec Hummingbird quadrotor are used to train our proposed models. (Right) Data from a Bitcraze Crazyflie2.0 quadrotor are used to validate the models.

A. Experimental Setup

1) Hummingbird Dataset: Experiments with AscTec Hummingbird are conducted in an 27 m L $\times$ 6.7 m W $\times$ 4.6 m H indoor robot testing area. The propeller radius is $R = 0.1$ m. The total mass is $m = 0.551$ kg. We consider eleven distinct forward velocities ($V \in \{0, 0.5, 1, 1.5, 2, 3, 4, 5, 6, 7, 8\}$ m/s ; $V = 0$ m/s corresponds to hover), and eight IGE altitudes ($z \in \{0.05, 0.1, 0.15, 0.2, 0.25, 0.3, 0.4, 0.5\}$ m).[1] A PD controller is used to track desired trajectories. To avoid crashing to the ground at high speeds due to large attitude, we remove altitudes lower than 0.1 m, 0.15 m, and 0.2 m from 6 m/s, 7 m/s, and 8 m/s flights, respectively. This leads to a total of 82 distinct case studies. For each case study, we collect 20 experimental trials. To account for variations that may exist (e.g., due to noise) but are hard to model and/or predict, we first perform variance reduction by averaging over the temporal duration of a constant velocity trajectory segment in each trial, and then averaging over all trials for each case study. The outcome is then used to train the proposed models.

We generate minimum-snap energy efficient trajectories [31], [32] (Fig. 2) for Hummingbird. Each trajectory is designed to have two key segments, an IGE and an OGE segment. We maximize the duration of constant velocity segments while adhering to workspace restrictions, which requires large accelerations at the beginning and at the end of each segment. However, large accelerations are difficult to achieve since they require large attitude changes, which could result in the arms of the robot contacting the ground. To mitigate this, when entering and exiting the IGE segments, the robot starts higher than the nominal IGE height and descends while accelerating laterally. In Fig. 2, starting from position ①, the vehicle accelerates to reach the desired velocity V and height z at position ②. Then, the vehicle moves forward in a straight line from position ② to ③ at constant velocity V and constant height z. From position ③, the vehicle starts to decelerate and rest at position ④. Later on, the vehicle follows similar process along positions ④, ⑤, ⑥, ①, with height at ⑤ and ⑥ being set at $z = 1$ m. The ground effect can be significant up to $5R$ above the ground for multi-rotor vehicles [19]–[21]. The return trajectory at $z = 1$ m satisfies the OGE condition.

[1]These are the commanded altitudes and forward velocities; actual values may vary due to process noise and measurement errors.

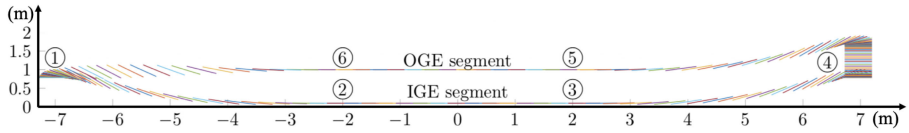

Fig. 2. Sample experimental trajectory designed offline.

2) Crazyflie Dataset: Experiments with a Crazyflie are conducted in a different, 7 m L × 5.5 m W × 3 m H indoor robot testing area. The propeller radius is $R = 0.023$ m. The total mass of the vehicle is $m = 0.032$ kg.

As the size of Crazyflie is much smaller compared with Hummingbird, it is reasonable to non-dimensionalize the commanded altitude and forward velocity. Doing so facilitates more direct comparisons between the two robots. We use two non-dimensional quantities: 1) the ratio of altitude to propeller radius, that is, $\frac{z}{R}$, and 2) the ratio of forward velocity to induced velocity at hover, that is, $\frac{V}{v_h}$. Operating conditions for Crazyflie are thus determined based on non-dimensionalized altitudes and velocities of Hummingbird. Due to the limitation of maximum velocity for Crazyflie and the constrained size of testing area, we choose five distinct forward velocities $V \in \{0, 0.52, 1.05, 1.57, 2.10\}$ m/s (corresponding to $V \in \{0, 0.5, 1, 1.5, 2\}$ m/s for Hummingbird), and six IGE altitudes $z \in \{0.035, 0.046, 0.058, 0.069, 0.092, 0.115\}$ m (corresponding to $z \in \{0.15, 0.2, 0.25, 0.3, 0.4, 0.5\}$ m for Hummingbird). Further, we add the OGE altitude, set at 1 m. This leads to a total of 35 distinct case studies. For each case study, we collect 20 experimental trials. The Crazyflie follows straight-line trajectories. A geometric controller [31], [33] is used to track desired trajectories with the Crazyflie.

B. Analysis of Experimental Data

Experimental trials are parameterized based on the UAV's forward velocity and altitude. To quantify the produced rotor thrust along a trajectory, one can follow the aerodynamic equations commonly used in rotorcraft [7]

$$T = 2\rho_a A v_i \sqrt{(v_\infty \cos\alpha)^2 + (v_\infty \sin\alpha + v_i)^2}, \tag{1}$$

where ρ_a is the density of air, α is the angle of attack, v_∞ and v_i are the free-stream velocity and induced velocity, respectively. Note that $v_\infty = 0$ at hover. Next, the induced velocity[2] in forward flight, v_i, can be found as [7]

$$v_i = \frac{v_h^2}{\sqrt{(v_\infty \cos\alpha)^2 + (v_\infty \sin\alpha + v_i)^2}}, \tag{2}$$

where v_h is the induced velocity at hover given by

$$v_h = \sqrt{\frac{T_{h,r}}{2\rho_a \pi R^2}}. \tag{3}$$

Term $T_{h,r}$ is the required thrust to hover for a single rotor; under ideal conditions it equals $mg/4$ for a quadrotor of mass m. We denote the thrust produced by each propeller in OGE and IGE, T_{OGE} and T_{IGE}, respectively. Note that instead of applying (1), thrust is directly calculated from experimental data. To create the models (based on Hummingbird data) we use rotor RPM values reported by the vehicles firmware to calculate the thrust as per $T = k_f \omega^2$. Thrust coefficient k_f for Hummingbird is found experimentally and set at $5.95 \cdot 10^{-8}$ N/RPM^2. For Crazyflie, we calculate thrust by directly converting consumed motor power per the manufacturer's power-thrust curves.

Figure 3(a) depicts T_{OGE} as forward velocity V varies for Hummingbird. The solid line (in red) indicates thrust at hover $T_h = mg$; marks (in blue) depict the average OGE thrust. We observe that the thrust remains practically constant when V/v_h is in the range $[0, 0.7]$. As forward velocity increases, the vehicle pitches forward more, the angle of attack increases, and the rotor induced velocity increases as per (2). Produced rotor thrust increases as per (1), thus decreasing the required thrust the flight controller needs to command. When $V/v_h > 0.7$, T_{OGE} starts to decrease. Thrust keeps decreasing and reaches curve minima around $V/v_h = 1.4$. When $V/v_h > 1.4$, thrust increases again. One explanation is that when forward velocity increases over $V/v_h > 1.4$, drag dominates and cancels the effect of increased induced velocity [34], [35]; more thrust is required to maintain constant OGE forward velocity.

Analysis in Section V is based on the ratio T_{IGE}/T_h. It has been found [17] that the rotor thrust increases for given power as it approaches the ground due to ground effect. Under the constant-power assumption, some existing models [18], [23] look into the ratio of thrust OGE to thrust IGE, T_{IGE}/T_{OGE}, with respect to the ratio z/R. Those models focus on ground effect at hover. At OGE hover, ideally $T_{OGE} = T_h = mg$; hence, T_{OGE} is constant through the studies, and these models indeed study T_{IGE}/T_h. However, when the vehicle moves forward, the required thrust varies during the entire flight due to feedback control. Figure 3(b) depicts T_{IGE}/T_{OGE} as V varies for Hummingbird. In principle, T_{OGE} should be the same for a given forward velocity (recall commanded trajectories in Fig. 2). However, small variations due to noise and measurement errors on T_{OGE} lead to improper noise magnification in the T_{IGE}/T_{OGE} ratio representation.

Figure 3(c) shows $T_{IGE}/T_h = T_{IGE}/mg$ with respect to forward velocity for different heights to ground. The ratio decreases as V increases, then starts to increase again around $V/v_h = 1.4$, where drag appears to begin to dominate, which is consistent with flight OGE (cf. Fig. 3(a)).

IV. Evaluation of Existing Models

The *Cheeseman & Bennett* model [17] considers forward velocity and distance from the ground for a single rotor, while other models [14], [18], [23] involve only hover. In this section, we examine the suitability of those four models for small-scale quadrotors operating IGE in forward flight.

[2]We note here that we implicit follow results based on Momentum Theory, and assume uniform induced velocity at hover and forward flight. Possible inaccuracies may be caused over aggressive maneuvers when the angle of attack is large. In this case, more accurate expressions may be used based on Blade Element (Momentum) Theory.

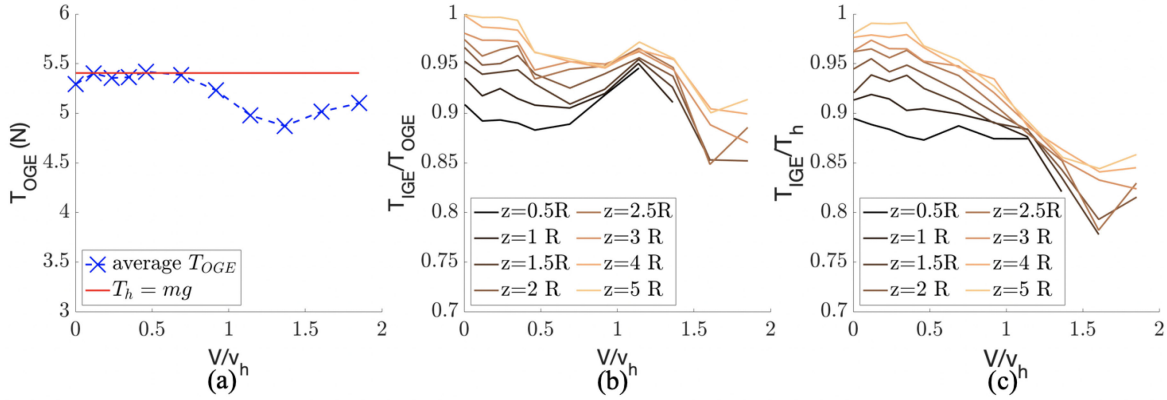

Fig. 3. Graphs of (a) OGE thrust; (b) IGE to OGE thrust ratio; and (c) IGE to thrust at hover, as forward velocity varies for Hummingbird data.

Cheeseman & *Bennett* [17] express the rotor thrust in ground effect for helicopters at hover as

$$\frac{T_{IGE}}{T_{OGE}} = \frac{1}{1 - \frac{(R/4z)^2}{1+(|V|/v_i)^2}}. \tag{4}$$

Hayden's [18] experimental model suggests

$$\frac{T_{IGE}}{T_{OGE}} = \left(0.9926 + \frac{0.03794}{(z/2R)^2}\right)^{2/3}. \tag{5}$$

Li et al. [14] introduce a correction coefficient

$$\frac{T_{input}}{T_{output}} = 1 - \rho\left(\frac{R}{4z}\right)^2, \tag{6}$$

where T_{input} is the commanded thrust, T_{output} is the actual thrust generated by the quadrotor, and ρ is a coefficient determined experimentally. T_{output} is expected to be greater than T_{input} under ground effect.

For the case of a quadrotor with a separation d from each rotor axis, the resultant expression for the ratio proposed by Sanchez-Cuevas *et al.* [23] is

$$\begin{aligned}\frac{T_{IGE}}{T_{OGE}} = {} & (1 - (R/4z)^2 - R^2\left(z/\sqrt{(d^2+4z^2)^3}\right) \\ & - (R^2/2)\left(z/\sqrt{2d^2+4z^2}\right)^3 \\ & - 2R^2\left(z/\sqrt{(b^2+4z^2)^3}K_b\right)^{-1},\end{aligned} \tag{7}$$

where b is the diagonal distance between two opposite rotor axes, and $K_b = 2$ is the empirical body lift coefficient. The term containing K_b accounts for flow recirculation and the central body lift that it generates.

A. Results of Fitting Existing Models

We evaluate existing models with data collected from the Hummingbird. First, we evaluate (4), which considers both altitude and forward velocity [17]. In Fig. 4(a), dashed curves with 'x' markers show the results from our experiments; forward velocity increases as color changes from brown to orange. Solid curves (in shades of blue) show the predicted T_{IGE}/T_{OGE} using *Cheeseman & Bennett*'s model; forward velocity increases as color changes from dark blue to cyan. The model predicts

TABLE I
IDENTIFIED COEFFICIENTS k AND b IN (8) FOR VARYING V

V/v_h	**0**	**0.12**	**0.24**	**0.35**	**0.47**	**0.71**
k_i	1.680	2.128	2.135	2.659	2.542	1.602
b_i	0.985	0.996	0.989	0.996	0.979	0.956
V/v_h	**0.95**	**1.18**	**1.47**	**1.65**	**1.89**	
k_i	2.010	0.591	3.597	4.300	-1.839	
b_i	0.938	0.898	0.886	0.889	0.898	

that ground effect diminishes as forward velocity increases. Results indicate (cf. [19]–[21]) that the influence of the ground is apparent up to heights of $z = 5R$, which is much higher than classic predictions [17]. Even though experimental results agree with the general trend of (4), the existence of offsets show that *Cheeseman & Bennett*'s model predicts higher required thrust. The solid curve with circular markers (in red) shows the predicted T_{IGE}/T_{OGE} using *Hayden*'s model. Since this model is extracted from test data, it fits the trend at hover, but it does not consider the influence of forward velocity.

Li et al. [14] identify the coefficient ρ in (6) at 8.6 with hover experiments at different altitudes. The solid curve with circular markers (in blue) in Fig. 4(b) shows the fitting of (6) to our experimental data. The trend of (6) does not agree with our experiment results. Fitting our experimental data to (6) gives $\rho^* = 3.4$. The plot with $\rho^* = 3.4$ is shown in Fig. 4(b) via the solid curve with square markers (in red). Results show that this model works well at hover, however, it still does not describe the influence of forward velocity.

Next, we examine a model in the general form of (6), i.e.

$$\frac{T_{input}}{T_{output}} = b_i - k_i\left(R/4z\right)^2, \tag{8}$$

to fit the experimental data. Different parameters k_i and b_i are determined for different forward velocities. Identified values of k_i and b_i are given in Table I. Fitting results are plotted in Fig. 4(c). The problem with (8) is that it fails to involve both z and V as variables.

Results of fitting model (7) to data are given in Fig. 4(a) with square markers (in green). The model does not consider forward velocity, and thus it is not surprising that it cannot describe ground effect in forward flight.

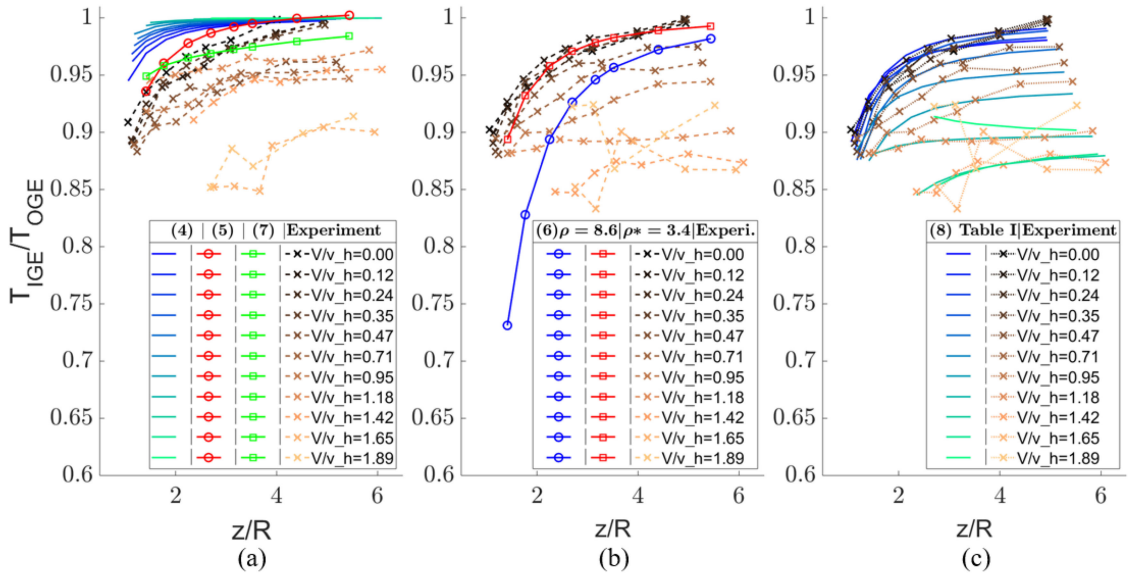

Fig. 4. (a) Evaluation of *Cheeseman & Bennett* (4), *Hayden* (5), and *Sanchez-Cuevas et al.* (7) models. (b) Evaluation of *Li et al.* model (6) when $\rho = 8.6$ and $\rho^* = 3.4$. (c) Evaluation of modified *Li et al.* model (8) with velocity-specific coefficients k_i and b_i. Note that (5), (6), and (7) do not depend on forward velocity. All evaluations use data collected with the AscTec Hummingbird quadrotor.

Our analysis indicates that existing models [14], [17], [18], [23] cannot fully describe the rotor performance for a multi-rotor vehicle in forward flight and in proximity to the ground.

V. Proposed Models

We propose two new models for analyzing produced thrust under the influence of ground effect in both hover and forward flight. Model structures are determined by the Buckingham Π method [36], and parameter values are identified via least squares optimization with data from Hummingbird. Our proposed models are evaluated and validated against data from Crazyflie. Note that the thrust, altitude, and forward velocity used in both fitting and evaluation use measured values. This helps remove dependence on the specific type of controller employed. We take average over trials to reduce variance.

Figure 4 shows that curves for lower forward velocities tend to cluster and be smoother than their higher speed counterparts. This evidence suggests that the ground effect exhibits a much stronger dependency on the altitude compared to forward velocity, within the range of low to medium forward velocities. Further, results from first-principles based modeling [35] suggest that around 8 m/s the required thrust should increase. Detailed aerodynamics analysis suggests that translational drag becomes more pronounced as forward velocity increases over a threshold [34]. Without considering ground effect, a data-driven model [37] is proposed to represent thrust (includes both real thrust generated by propellers and drag force acting on the frame and rotors) as third order polynomial with respect to forward velocity. Inspired by these findings, for each of our proposed models we provide separate forms for i) low/medium forward velocity, and ii) high forward velocity.

The functional expression of thrust in terms of altitude z and forward velocity V is found by non-dimensional analysis:

$$f(T_{IGE}, T_h, R, z, V, v_h) = 0. \tag{9}$$

According to the Buckingham Π method [36], we select z, v_h and T_h to be independent variables, and (9) becomes

$$\frac{T_{IGE}}{T_h} = f_1\left(\frac{V}{v_h}, \frac{R}{z}\right). \tag{10}$$

We test several combinations of V/v_h and R/z terms and their powers. To avoid overfitting, we seek to identify the simplest possible structures that best explain the data.

A. Proposed Model 1

Model 1 builds on top of the structure of (10). We split the velocity into two groups, $V/v_h \in [0, 1.2]$ is considered low-to-medium speed, $V/v_h > 1.2$ is considered high speed.

1) Low/Medium Speed Flight: We propose

$$\frac{T_{IGE}}{T_h} = \frac{1 - \frac{3R}{25z}}{1 + \frac{3}{50}(\frac{V}{v_h})^3}. \tag{11}$$

This form includes a term of higher than second order polynomial for V, which agrees with analytical [34], [35] and experimental [5], [37] results. As z increases, the vehicle is less influenced by ground effect, thus T_{IGE}/T_h increases. As V increases, the induced velocity increases, hence less thrust is required and T_{IGE}/T_h decreases. At hover,

$$T_{IGE} = T_h\left(1 - \frac{3R}{25z}\right) = mg\left(1 - \frac{3R}{25z}\right), \tag{12}$$

and (12) agrees with previous studies in the sense that the required thrust varies based on the vehicle's distance from the ground. When $z > 5R$, $\frac{3R}{25z} < 0.024$, and $T_{IGE} \approx T_h$.

Fitting Model 1 for low/medium velocity is given in Fig. 5. Solid curves (in black) with 'x' markers denote the results calculated by using the measured velocity from motion capture and the calculated thrust based on reported RPM values. One standard deviation bounds are shown with light gray background. Dashed curves with circular markers (in orange) show the predicted

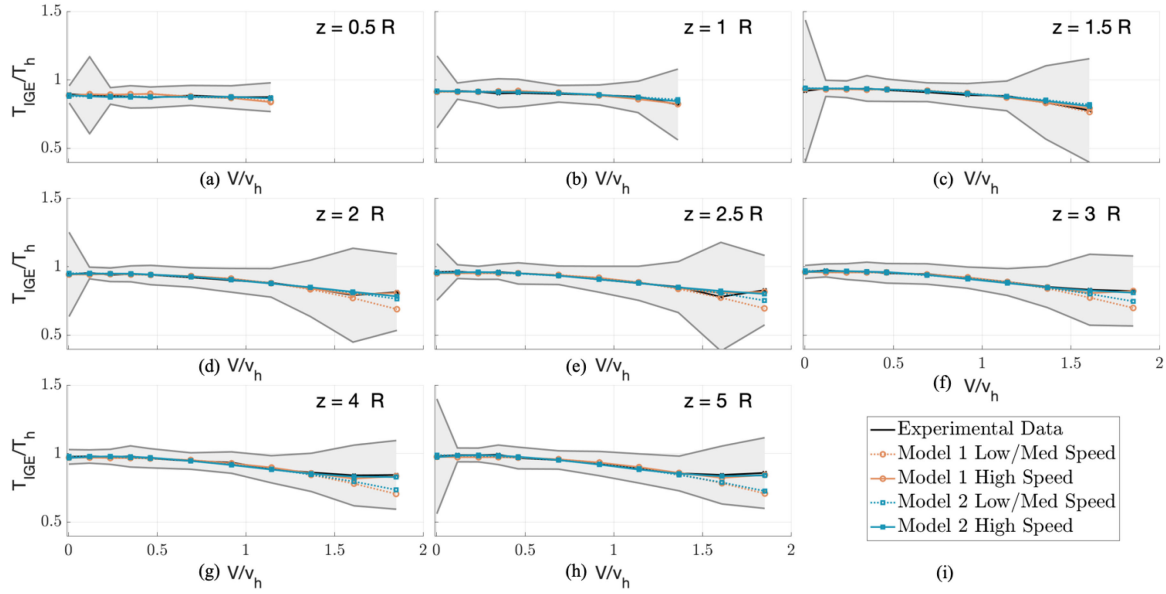

Fig. 5. Plots of fitting Model 1 low and medium speed (dashed orange), Model 1 high speed (solid orange), Model 2 low and medium speed (dashed blue), and Model 2 high speed (solid blue) flights. Mean (solid black with markers) and standard deviation (shaded grey) of experimental data over 20 trials are given. (a)–(h) represent the distance to ground in the range of [0.5R 5R], (i) is the legend for (a)–(h).

TABLE II
RMSE AND MAE OF MODEL FITTING FOR HUMMINGBIRD AND PREDICTION FOR CRAZYFLIE

		Hummingbird								Crazyflie					
Model	**z/R**	**0.5**	**1.0**	**1.5**	**2.0**	**2.5**	**3.0**	**4.0**	**5.0**	**1.5**	**2.0**	**2.5**	**3.0**	**4.0**	**5.0**
#1 Low	rmse	0.016	0.009	0.010	0.007	0.008	0.006	0.008	0.011	0.008	0.006	0.009	0.009	0.016	0.018
	mae	0.013	0.007	0.009	0.006	0.007	0.005	0.007	0.009	0.007	0.005	0.008	0.008	0.013	0.013
#1 High	rmse	0.018	0.009	0.010	0.007	0.011	0.009	0.011	0.013	0.008	0.006	0.009	0.009	0.016	0.018
	mae	0.015	0.007	0.009	0.006	0.009	0.006	0.009	0.011	0.007	0.005	0.008	0.008	0.013	0.013
#2 Low	rmse	0.008	0.004	0.007	0.004	0.005	0.006	0.006	0.007	0.015	0.006	0.009	0.006	0.015	0.017
	mae	0.007	0.003	0.006	0.004	0.004	0.005	0.004	0.006	0.014	0.005	0.008	0.006	0.011	0.011
#2 High	rmse	0.006	0.009	0.013	0.013	0.015	0.007	0.009	0.008	0.015	0.007	0.008	0.007	0.014	0.020
	mae	0.006	0.006	0.010	0.009	0.009	0.006	0.007	0.007	0.015	0.006	0.007	0.006	0.010	0.014

thrust from (11). The Root Mean Squared Error (RMSE) and Mean Absolute Error (MAE) for fitting (11) to experimental data are given in Table II.

2) High Speed Flight: As velocity increases, drag starts to dominate [34], [35] and thrust increases. To represent the influence of drag, we add a third order polynomial term in V:

$$\frac{T_{IGE}}{T_h} = \frac{1 - \frac{3R}{25z}}{1 - \frac{3}{50}\left(\frac{V}{v_h}\right)^3} - \frac{29}{250}\left(\frac{V}{v_h}\right)^3. \tag{13}$$

Fitting results for high speed flight in Fig. 5 are shown by solid curves with circular markers (in orange). Equation (13) predicts the trend of T_{IGE}/T_h as V increases, as well as the curve minima around $V/v_h = 1.4 - 1.6$.

The RMSE and MAE for predicting high speed flight performance using (13) are given in Table II. The table shows that (11) has slightly better overall prediction accuracy compared to (13). If this performance deficit is not particularly significant, one can apply (13) for predicting thrust IGE for all velocities up to $V/v_h = 1.9$. Models (11) and (13) both have best prediction accuracy when $z = 2R$, and worst at $z = 0.5R$. Data suggest that as the order of R/z increases, we get slightly better fit for flights at hover; as the order of V/v_h increases, we get better fit of the curve trends.

B. Proposed Model 2

For Model 2, we first consider thrust as a function of V/v_h, then fit the coefficients as a function of R/z. Similarly to Model 1, we also provide separate models for low and medium speed, and for high speed flight.

1) Low/Medium Speed Flight: In this case we propose

$$\frac{T_{IGE}}{T_h} = \left(0.104\frac{R}{z} - 0.0952\right)\left(\frac{V}{v_h}\right)^2 - 0.171\frac{R}{z} + 1.02. \tag{14}$$

Model 2 fitting results for low-to-medium-speed flight are given in Fig. 5 via dashed curves with square markers (in blue). Corresponding RMSE and MAE values are given in Table II.

Equation (14) has lower order term of V/v_h compared to (11). However, since the coefficient of $(\frac{V}{v_h})^2$ is a function of R/z, the trend of thrust change as V increases is less evident. At hover, (14) becomes $\frac{T_{IGE}}{T_h} = -0.171\frac{R}{z} + 1.02$, which is a function of height only, as desired.

2) High Speed Flight: The proposed expression now is

$$\frac{T_{IGE}}{T_h} = p_1 \left(\frac{V}{v_h}\right)^3 + p_2 \left(\frac{V}{v_h}\right)^2 + p_3 \left(\frac{V}{v_h}\right) + p_4. \quad (15)$$

Terms $p_1,\ p_2,\ p_3$, and p_4 are linear functions of R/z, where

$$\begin{aligned} p_1 &= -0.337 \left(\frac{R}{z}\right) + 0.161, \\ p_2 &= 0.773 \left(\frac{R}{z}\right) - 0.428, \\ p_3 &= -0.35 \left(\frac{R}{z}\right) + 0.182, \\ p_4 &= -0.135 \left(\frac{R}{z}\right) + 1. \end{aligned} \quad (16)$$

Term $(\frac{V}{v_h})^3$ describes the effect of increased drag, and agrees with reported results [34], [35] that consider higher-order terms for V. Fitting results for high speed flight using Model 2 are shown in Fig. 5 via solid curves with square markers (in blue). RMSE and MAE values for (15) are given in Table II.

Model 2 gives the best and the worst prediction accuracy at $z = 0.5R$ and $z = 2R$, respectively, for high speed flight. However, Model 2 does not reflect as clearly the curve increase around $V/v_h = 1.4 - 1.6$. The overall prediction error of Model 2 is less than the error of Model 1, which is expected since Model 2 has more parameters.

Each proposed model provides advantages in different situations. For Model 1, (13) offers a single function for predicting rotor performance for the whole velocity range, at the expense of accuracy. In both forms of Model 1, the terms that involve V and z are isolated. This simple expression enables direct estimation of thrust change due to altering velocity and height. In addition, Model 1 describes the decrease-increase curve trend and the minimal point more clearly compared to Model 2. The latter can better predict the IGE thrust for small distances from the ground. In Table II, Model 2 shows better overall performance for low and medium speed. Thus, when prediction accuracy is the main concern, Model 2 may be preferable. Furthermore, both high speed models indicate that, for $V/v_h > 1.88$, required thrust increases steadily. One explanation is that, for high velocity, higher-order drag effects begin to dominate [34], effectively canceling the positive effects of induced velocity and hence increasing required thrust.

C. Evaluation of Proposed Models

We validate the proposed models with the data collected from Crazyflie. Figure 6 shows the prediction results. In each subplot, dashed curves with 'x' markers show the results from our experiments; commanded altitude increases as color changes from brown to orange. Solid curves (in shades of blue) show the predicted T_{IGE}/T_h using (a) Model 1 low speed (11), (b) Model 1 high speed (13), (c) Model 2 low speed (14), (c) Model 2 high speed (15); commanded altitude increases as color changes from dark blue to cyan. The RMSE and MAE for prediction are given in Table II.

The result shows that proposed models fitted with Hummingbird data are able to predict T_{IGE}/T_h for another quadrotor in the case of different frame size, mass, trajectories, controller, and environment. Both low/medium speed and high speed versions of the models give similar predictions since collected data correspond to low/medium speed flight.

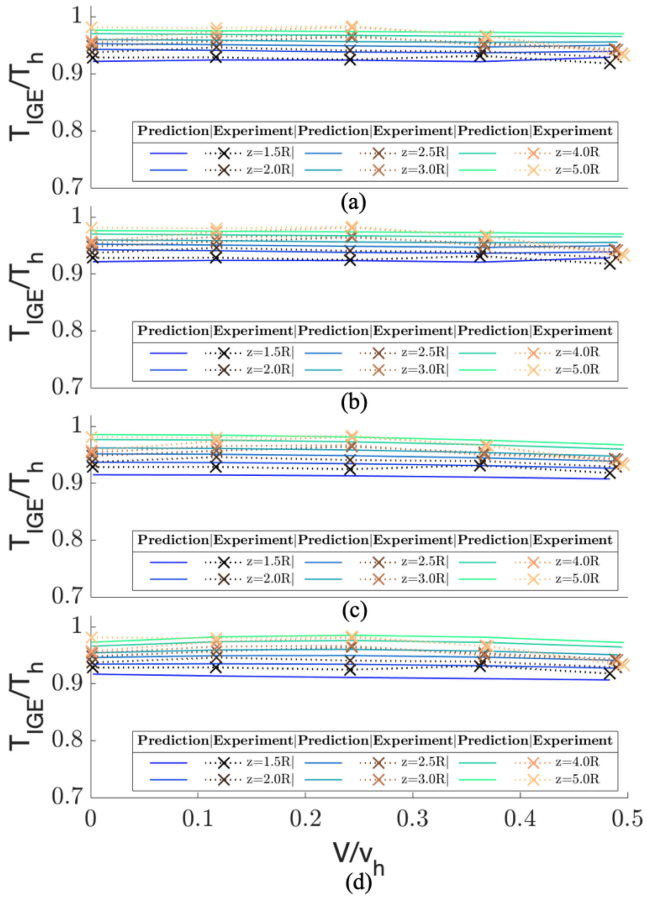

Fig. 6. Predicting Crazyflie T_{IGE}/T_h with (1) Model 1 Low Speed, (b) Model 1 High Speed, (c) Model 2 Low Speed, and (d) Model 2 High Speed.

VI. Conclusion

This letter proposes two new models to explain the impact of ground effect both at hover and in forward flight for small-scale rotorcraft UAVs. We evaluate the influence of vehicle forward velocity and altitude to ground effect. Extensive experiments under varying velocities and altitudes are conducted with two distinct quadrotor UAVs of different size and mass.

Collected data indicate that, for fixed altitude, the required thrust initially decreases, then reaches a curve minimum, and finally increases, as forward velocity increases. Existing ground effect models for helicopters or multirotors at hover fail to capture this phenomenon in forward flight.

To address this gap, we provide two new models that uniquely blend data-driven methods with non-dimensional analysis and first-principles aerodynamics. A key benefit of the proposed models is that they establish clear and intuitive relations between robot-relevant and operation-relevant parameters (e.g., induced velocity and rotor radius, and forward velocity and altitude, respectively). Taken together, the two models establish tradeoffs between model complexity, structure, and training/validation accuracy.

Both models are tested in hover and up to 8 m/s forward velocity. To capture observed curve minima as forward velocity increases, we provide two variants for each model: 1) a hover and low-to-medium-speed, and 2) a high-speed variant. The first variant is validated with data from a quadrotor of smaller size and lower weight. This finding enhances the generalization capability of our proposed models for quadrotor UAVs at hover and in low-to-medium-speed forward flight. Consistent with related work [5], [34], [35], [37] suggesting that as speed increases higher-order aerodynamic effects (e.g., drag) begin to dominate, a third order polynomial velocity term is included in high-speed variants. While robot and workspace constraints hindered validation of high-speed variants with the smaller quadrotor, we anticipate that our models can be enhanced with models aimed at capturing higher-ordered aerodynamic effects occurring as forward velocity increases (e.g., [34]) to better capture quadrotor behaviors in high-speed flight.

The work here contributes to promoting the understanding of how proximity to the ground affects the behavior of small-scale rotorcraft UAVs across various operating conditions in terms of altitude and forward velocity. This is the first study that captures ground effects through extensive indoor experimentation across several altitudes and forward velocities. Even though this work is grounded on quadrotors—one of the most prevalent type of UAV nowadays [38]—our findings may guide analysis of other multirotor vehicles with distinct number of rotors, or very different scaling among rotor radius, arm length, and frame shape. Other interesting directions of future research may include performing a CFD simulation to observe the behavior of the flow field and thus better link data-driven and physics-based approaches for modeling the impact aerodynamic effects on UAV behavior. Furthermore, the new knowledge created by this work may contribute to applications that involve near-ground operations in aerial manipulation and multi-robot systems.

REFERENCES

[1] H. Ma, C. Tovey, G. Sharon, T. Kumar, and S. Koenig, "Multi-agent path finding with payload transfers and the package-exchange robot-routing problem," in *Proc. 30th AAAI Conf. Artif. Intell.*, 2016, pp. 3166–3173.

[2] X. Jin, S. Liu, F. Baret, M. Hemerl, and A. Comar, "Estimates of plant density of wheat crops at emergence from very low altitude UAV imagery," *Remote Sens. Environ.*, vol. 198, pp. 105–114, 2017.

[3] F. Augugliaro *et al.*, "The flight assembled architecture installation: Cooperative construction with flying machines," *Control Syst.*, vol. 34, pp. 46–64, 2014.

[4] M. Beul, N. Krombach, M. Nieuwenhuisen, D. Droeschel, and S. Behnke, *Autonomous Navigation in a Warehouse With a Cognitive Micro Aerial Vehicle*. Berlin, Germany: Springer, 2017, pp. 487–524.

[5] J. Ware and N. Roy, "An analysis of wind field estimation and exploitation for quadrotor flight in the urban canopy layer," in *Proc. IEEE Int. Conf. Robot. Autom.*, 2016, pp. 1507–1514.

[6] K. Vicencio, T. Korras, K. A. Bordignon, and I. Gentilini, "Energy-optimal path planning for six-rotors on multi-target missions," in *Proc. IEEE/RSJ Int. Conf. Intell. Robots Syst.*, 2015, pp. 2481–2487.

[7] G. J. Leishman, *Principles of Helicopter Aerodynamics*. Cambridge, U.K.: Cambridge Univ. Press, 2006.

[8] M. Ryll, H. H. Blthoff, and P. R. Giordano, "A novel overactuated quadrotor unmanned aerial vehicle: Modeling, control, and experimental validation," *IEEE Trans. Control Syst. Technol.*, vol. 23, no. 2, pp. 540–556, Mar. 2015.

[9] F. Morbidi, R. Cano, and D. Lara, "Minimum-energy path generation for a quadrotor UAV," in *Proc. IEEE Int. Conf. Robot. Autom.*, 2016, pp. 1492–1498.

[10] A. Koehl, H. Rafaralahy, M. Boutayeb, and B. Martinez, "Aerodynamic modelling and experimental identification of a coaxial-rotor UAV," *J. Intell. Robotic Syst.*, vol. 68, no. 1, pp. 53–68, Sep. 2012.

[11] M. Schulz, F. Augugliaro, R. Ritz, and R. D'Andrea, "High-speed, steady flight with a quadrocopter in a confined environment using a tether," in *Proc. IEEE/RSJ Int. Conf. Intell. Robots Syst.*, 2015, pp. 1279–1284.

[12] M. Debord, W. Hönig, and N. Ayanian, "Trajectory planning for heterogeneous robot teams," in *Proc. IEEE/RSJ Int. Conf. Intell. Robots Syst.*, 2018, pp. 7924–7931.

[13] J. A. Preiss, W. Hönig, N. Ayanian, and G. S. Sukhatme, "Downwash-aware trajectory planning for large quadrotor teams," in *Proc. IEEE Int. Conf. Intell. Robots Syst.*, 2017, pp. 250–257.

[14] D. Li, Y. Zhou, Z. Shi, and G. Lu, "Autonomous landing of quadrotor based on ground effect modelling," in *Proc. 34th Chin. Control Conf.*, 2015, pp. 5647–5652.

[15] J. Thomas *et al.*, "Planning and control of aggressive maneuvers for perching on inclined and vertical surfaces," in *Proc. Int. Design Eng. Tech. Conf. Comput. Inf. Eng. Conf.*, Boston, MA, USA, 2015, p. V05CT08A012.

[16] K. Mohta *et al.*, "Fast, autonomous flight in GPS-denied and cluttered environments," *J. Field Robot.*, vol. 35, no. 1, pp. 101–120, 2018.

[17] I. C. Cheeseman and W. E. Bennett, "The effect of ground on a helicopter rotor in forward flight," Aeronaut. Res. Council, London, U.K., Tech. Rep. RM No. 3021, 1955.

[18] J. S. Hayden, "The effect of the ground on helicopter hovering power required," in *Proc. 32th Annu. Nat. Forum Amer. Helicopter Soc.*, Washington, DC, USA, May 1976.

[19] C. Powers, D. Mellinger, A. Kushleyev, B. Kothmann, and V. Kumar, "Influence of aerodynamics and proximity effects in quadrotor flight," in *Proc. Exp. Robot.: 13th Int. Symp. Exp. Robot.*, 2013, pp. 289–302.

[20] I. Sharf *et al.*, "Ground effect experiments and model validation with Draganflyer X8 rotorcraft," in *Proc. Int. Conf. Unmanned Aircr. Syst.*, Orlando, FL, USA, 2014, pp. 115–1166.

[21] D. Del Cont Bernard, F. Riccardi, M. Giurato, and M. Lovera, "A dynamic analysis of ground effect for a quadrotor platform," in *Proc. 20th IFAC World Congress*, Toulouse, France, 2017, pp. 10311–10316.

[22] D. A. Griffiths and G. Leishman, "A study of dual-rotor interference and ground effect using a free-vortex wake model," in *Proc. 58th Annu. Nat. Forum Amer. Helicopter Soc.*, vol. 1, pp. 59–612, 2002.

[23] P. Sanchez-Cuevas, G. Heredia, and A. Ollero, "Characterization of the aerodynamic ground effect and its influence in multirotor control," *Int. J. Aerosp. Eng.*, vol. 2017, 2017, Art. no. 1823056.

[24] K. Karydis and M. A. Hsieh, "Uncertainty quantification for small robots using principal orthogonal decomposition," in *Proc. Int. Symp. Exp. Robot.*, 2016, pp. 33–42.

[25] M. Loeve, *Probability Theory*. Princeton, NJ, USA: Van Nostrand, 1955.

[26] K. Karydis, I. Poulakakis, J. Sun, and H. G. Tanner, "Probabilistically valid stochastic extensions of deterministic models for systems with uncertainty," *Int. J. Robot. Res.*, vol. 34, no. 10, pp. 1278–1295, 2015.

[27] A. Graber, A. Rosen, and A. Seginer, "An investigation of a hovering rotor in ground effect," in *Proc. 16th Eur. Rotorcraft Forum*, Glasgow, Scotland, 1990, pp. 161–169.

[28] N. Itoga, N. Iboshi, M. Horimoto, S. Saito, and Y. Tanabe, "Numerical analysis of helicopter rotor hovering in close proximity to the ground with a wall," *J. Jpn. Soc. Aeronaut. Space Sci.*, vol. 58, pp. 269–276, 2010.

[29] J. Xin, R. Chen, and P. Li, "Time-stepping free-wake methodology for rotor flow field simulation in ground effect," *Aircr. Eng. Aerosp. Technol.*, vol. 87, no. 5, pp. 418–426, 2015.

[30] K. Yu and D. A. Peters, "Nonlinear statespace modeling of dynamic ground effect," *J. Amer. Helicopter Soc.*, vol. 50, no. 3, pp. 259–268, 2005.

[31] D. Mellinger and V. Kumar, "Minimum snap trajectory generation and control for quadrotors," in *Proc. IEEE Int. Conf. Robot. Autom.*, 2011, pp. 2520–2525.

[32] N. Kreciglowa, K. Karydis, and V. Kumar, "Energy efficiency of trajectory generation methods for stop-and-go aerial robot navigation," in *Proc. Int. Conf. Unmanned Aircr. Syst.*, 2017, pp. 656–662.

[33] T. Lee, M. Leok, and N. H. McClamroch, "Geometric tracking control of a quadrotor UAV on SE(3)," in *Proc. 49th IEEE Conf. Decis. Control*, 2010, pp. 5420–5425.

[34] M. Bangura and R. Mahony, "Nonlinear dynamic modeling for high performance control of a quadrotor," in *Proc. Australas. Conf. Robot. Autom.*, Wellington, New Zealand, 2012, pp. 115–124.

[35] R. Gill and R. D'Andrea, "Propeller thrust and drag in forward flight," in *Proc. IEEE Conf. Control Technol. Appl.*, 2017, pp. 73–79.

[36] E. Buckingham, "On physically similar system; illustrations of the use of dimensional equations," *Phys. Rev.*, vol. 4, pp. 345–376, Oct. 1914.

[37] S. Sun, C. De Visser, and Q. Chu, "Quadrotor gray-box model identification from high-speed flight data," *J. Aircr.*, vol. 56, pp. 645–661, 2019.

[38] K. Karydis and V. Kumar, "Energetics in robotic flight at small scales," *Roy. Soc. Interface Focus*, vol. 7, no. 1, 2017, Art. no. 20160088.